J|A|C|S
ARTICLES
Published on Web 05/20/2004

Synthesis, Photophysics, Electrochemistry, Theoretical, and Transient Absorption Studies of Luminescent Copper(I) and Silver(I) Diynyl Complexes. X-ray Crystal Structures of $[Cu_3(\mu\text{-dppm})_3(\mu_3\text{-}\eta^1\text{-}C{\equiv}CC{\equiv}CPh)_2]PF_6$ and $[Cu_3(\mu\text{-dppm})_3(\mu_3\text{-}\eta^1\text{-}C{\equiv}CC{\equiv}CH)_2]PF_6$

Wing-Yin Lo,[†] Chi-Ho Lam,[†] Vivian Wing-Wah Yam,*[,†] Nianyong Zhu,[†] Kung-Kai Cheung,[†] Sofiane Fathallah,[‡] Sabri Messaoudi,[‡] Boris Le Guennic,[‡] Samia Kahlal,[‡] and Jean-François Halet*[,‡]

Contribution from the Centre for Carbon-Rich Molecular and Nano-Scale Metal-Based Materials Research, Department of Chemistry, and HKU-CAS Joint Laboratory of New Materials, The University of Hong Kong, Pokfulam Road, Hong Kong SAR, People's Republic of China, and Laboratoire de Chimie du Solide et Inorganique Moléculaire, UMR 6511 CNRS-Université de Rennes 1, Institut de Chimie de Rennes, Campus de Beaulieu, F-35042 Rennes, France

Received February 9, 2004; E-mail: wwyam@hku.hk; halet@univ-rennes1.fr

Abstract: A series of soluble trinuclear copper(I) and silver(I) complexes containing bicapped diynyl ligands, $[M_3(\mu\text{-dppm})_3(\mu_3\text{-}\eta^1\text{-}C{\equiv}CC{\equiv}CR)_2]PF_6$ (M = Cu, R = Ph, C_6H_4—CH_3-*p*, C_6H_4—OCH_3-*p*, $^nC_6H_{13}$, H; M = Ag, R = Ph, C_6H_4—OCH_3-*p*), has been synthesized and their electronic, photophysical, and electrochemical properties studied. The X-ray crystal structures of $[Cu_3(\mu\text{-dppm})_3(\mu_3\text{-}\eta^1\text{-}C{\equiv}CC{\equiv}CPh)_2]PF_6$ and $[Cu_3(\mu\text{-dppm})_3(\mu_3\text{-}\eta^1\text{-}C{\equiv}CC{\equiv}CH)_2]PF_6$ have been determined.

Introduction

Recent interests in metal alkynyl chemistry were stimulated by the increasing attention on polymeric materials with polarizable moieties for the fabrication of electronic, liquid crystal, and nonlinear optical (NLO) devices.[1−6] The linear geometry of the poly-ynyl unit and its π-unsaturated nature have made the metal poly-ynes attractive building blocks for molecular wires and organometallic oligomeric and polymeric materials which may possess unique properties such as optical nonlinearity, electrical conductivity, and liquid crystallinity.[7−11] The photoluminescence properties of metal-containing oligoynes and poly-ynes are relatively less explored. Recently, we reported the syntheses and the luminescence studies of trinuclear monoynyl copper(I) and silver(I) diphosphine complexes,[12,13] and tetranuclear copper(I) complexes containing the mono-[13,14] and diynyl moieties.[15] As an extension of the work on the monoynyl trinuclear copper(I) and silver(I) complexes, a series of trinuclear copper(I) and silver(I) complexes of the diynyl

[†] The University of Hong of Kong.
[‡] Université de Rennes 1.

(1) (a) Yam, V. W. W. *Chem. Commun*. **2001**, 789. (b) Dembinski, R.; Lis, T.; Szafert, S.; Mayne, C. L.; Bartik, T.; Gladysz, J. A. *J. Organomet. Chem*. **1999**, *578*, 229. (c) Cifuentes, M. P.; Driver, J.; Humphrey, M. G.; Asselberghs, I.; Persoons, A.; Samoc, M.; Luther-Daview, B. *J. Organomet. Chem*. **2000**, *607*, 72. (d) Fyfe, H. B.; Mlekuz, M.; Stringer, G.; Taylor, N. J.; Marder, T. B. In *Inorganic and Organometallic Polymers with Special Properties*; Laine, R. M., Ed.; Kluwer: Dordrecht, 1992; pp 331−334. (e) Fyfe, H. B.; Mlekuz, M.; Zargarian, D.; Taylor, N. J.; Marder, T. B. *J. Chem. Soc., Chem. Commun*. **1991**, 188. (f) Fyfe, H. B.; Mlekuz, M.; Zargarian, D.; Marder, T. B. *Organometallics* **1991**, *10*, 204.
(2) (a) Corriu, R. J. P.; Douglas, W. E.; Yang, Z. X.; Karakus, Y.; Cross, G. H.; Bloor D. *J. Organomet. Chem.* **1993**, *455*, 69. (b) Long, N. J. *Angew. Chem., Int. Ed. Engl*. **1995**, *34*, 21.
(3) (a) Altmann, M.; Enkelmann, V.; Lieser, G.; Bunz, U. H. F. *Adv. Mater*. **1995**, *7*, 726. (b) Altmann, M.; Bunz, U. H. F. *Angew. Chem., Int. Ed. Engl*. **1995**, *34*, 569. (c) Faulkner, C. W.; Ingham, S. L.; Khan, M. S.; Lewis, J.; Long, N. J.; Raithby, P. R. *J. Organomet. Chem*. **1994**, *482*, 139. (d) Sonogashira, K.; Ohga, K.; Takahashi, S.; Hagihara, N. *J. Organomet. Chem*. **1980**, *188*, 237.
(4) (a) Nishihara, H.; Shimura, T.; Ohkubo, A.; Matsuda, N.; Aramaki, K. *Adv. Mater*. **1993**, *5*, 752. (b) Stiegman, A. E.; Miskowski, V. M.; Perry, J. W.; Coulter, D. R. *J. Am. Chem. Soc*. **1987**, *109*, 5884.
(5) Takahashi, S.; Takai, Y.; Morimoto, H.; Sonogashira, K.; Hagihara, N. *Mol. Cryst. Liq. Cryst*. **1982**, *32*, 139.
(6) Atherton, Z.; Faulkner, C. W.; Ingham, S. L.; Kakkar, A. K.; Khan, M. S.; Lewis, J.; Long, N. J.; Raithby, P. R. *J. Organomet. Chem*. **1993**, *462*, 265 and references therein.
(7) (a) Muller, T. J. J.; Lindner, H. J. *Chem. Ber*. **1996**, *129*, 607. (b) Brédas J.-L., Chance, R. R., Eds. *Conjugated Polymer Materials Opportunities in Electronic, Optoelectronic and Molecular Electronics*; NATO ASI Series; Kluwer: Dordrecht, 1990; Vol. 182.
(8) (a) Davey, A. P.; Cardin, D. J.; Byrne, H. J.; Blau, W. J. In *Inorganic Molecules For Nonlinear Optics and Photonics*; Messier, J., Prasad, P., Ulrich, D., Eds.; Kluwer: Dordrecht, The Netherlands, 1991; p 391. (b) Blau, W. J.; Byrne, H. J.; Cardin, D. J.; Davey, A. P. *J. Mater. Chem.* **1991**, *1*, 245.
(9) (a) Guha, S.; Frazier, C. C.; Porter, P. L.; Kang, K.; Finberg, S. E. *Opt. Lett*. **1989**, *14*, 952. (b) Frazier, C. C.; Guha, S.; Chen, W. P.; Cockerham, M. P.; Porter, P. L.; Chauchard, E. A.; Lee, C. H. *Polymer* **1987**, *28*, 553.
(10) (a) Takahashi, S.; Takai, Y.; Morimoto, H.; Sonogashira, K. *J. Chem. Soc., Chem. Commun.* **1984**, 3. (b) Takahashi, S.; Morimoto, H.; Murata, E.; Kataoka, S.; Sonogashira, K.; Hagihara, N. *J. Polym. Sci.: Polym. Chem. Ed*. **1982**, *20*, 565.
(11) (a) Ward, M. D. *Chem. Ind*. **1996**, 568. (b) Ward, M. D. *Chem. Ind*. **1997**, 640. (c) Astruc, D. *Acc. Chem. Res*. **1997**, *30*, 383.
(12) (a) Yam, V. W. W.; Lee, W. K.; Lai, T. F. *Organometallics* **1993**, *12*, 2383. (b) Yam, V. W. W.; Lee, W. K.; Yeung, P. K. Y.; Phillips, D. *J. Phys. Chem*. **1994**, *98*, 7545. (c) Yam, V. W. W.; Lee, W. K.; Cheung, K. K.; Crystall, B.; Phillips, D. *J. Chem. Soc., Dalton Trans*. **1996**, 3283. (d) Yam, V. W. W.; Fung, W. K. M.; Wong, M. T. *Organometallics* **1997**, *16*, 1772. (e) Yam V. W. W.; Fung, W. K. M.; Cheung, K. K. *Organometallics* **1997**, *16*, 2032. (f) Yam, V. W. W.; Fung, W. K. M.; Cheung, K. K. *Chem. Commun*. **1997**, 963. (g) Yam, V. W. W.; Fung, W. K. M.; Cheung, K. K. *Organometallics* **1998**, *17*, 3293.

 10.1021/ja049300x CCC: $27.50

systems have been synthesized, which would provide further insights into the spectroscopic origin of these classes of complexes. It is envisaged that such structural variation by a systematic extension of the acetylenic unit would not only provide a handle for the understanding of the spectroscopic studies of these complexes but also serve to produce new luminescent metal-based carbon-rich materials for applications in the future design and fabrication of light-emitting oligomeric and polymeric materials in materials science. Herein are described the synthesis, electronic structure, luminescence behavior, and electrochemistry of a series of trinuclear copper(I) and silver(I) diynyl complexes. The X-ray crystal structures of $[Cu_3(\mu\text{-dppm})_3(\mu_3\text{-}\eta^1\text{-}C{\equiv}CC{\equiv}CPh)_2]PF_6$ and $[Cu_3(\mu\text{-dppm})_3(\mu_3\text{-}\eta^1\text{-}C{\equiv}CC{\equiv}CH)_2]PF_6$ are also reported.

Experimental Section

Materials and Reagents. The ligands bis(diphenylphosphino)methane (dppm) was obtained from Lancaster Synthesis Ltd. 1,4-Bis(trimethylsilyl)-1,3-butadiyne was purchased from GFS Chemicals. $[Cu_2(\mu\text{-dppm})_2(MeCN)_2](PF_6)_2$[16a] and $[Ag_2(\mu\text{-dppm})_2(MeCN)_2](PF_6)_2$[16b] were prepared according to literature procedures. Phenylbutadiyne, 4-tolylbutadiyne, 4-methoxyphenylbutadiyne,[17] and 1,3-decadiyne[18] were synthesized by reported procedures. All solvents were purified and distilled using standard procedures before use.[19a] All other reagents were of analytical grade and were used as received. The pyridinium acceptors were prepared by refluxing the corresponding substituted pyridine with the appropriate alkylating agent such as methyl iodide in acetone/ethanol (1:1 v/v) for 4 h, followed by metathesis in water using ammonium hexafluorophosphate and recrystallization from acetone-diethyl ether. Tetra-*n*-butylammonium hexafluorophosphate (Aldrich) was recrystallized twice from absolute ethanol before use.

Syntheses of Trinuclear Copper(I) Complexes. All reactions were carried out under anaerobic and anhydrous conditions using standard Schlenk techniques.

$[Cu_3(\mu\text{-dppm})_3(\mu_3\text{-}\eta^1\text{-}C{\equiv}C{-}C{\equiv}C{-}Ph)_2]PF_6$ (1). A mixture of $[Cu_2(\mu\text{-dppm})_2(MeCN)_2](PF_6)_2$ (0.11 g, 0.09 mmol) and HC≡C−C≡C−Ph (0.03 g, 0.24 mmol) in the presence of an excess of KOH in acetone/MeOH (15 mL/5 mL) was stirred at room temperature for 24 h. After evaporation to dryness, the solid residue was extracted with CH_2Cl_2. Subsequent diffusion of diethyl ether vapor into the concentrated solution resulted in the formation of yellow crystals of **1**. Yield: 0.09 g (87%). Alternatively, replacement of KOH by triethylamine also gave the desired product but in a slightly lower yield. UV/vis (CH_2Cl_2), λ/nm (ϵ_{max}/dm^3 mol^{-1} cm^{-1}): 264 (80 010), 296sh (72 800), 338sh (33 350). Raman (solid), ν/cm^{-1}: 1980s, 2163s [ν(C≡C−C≡C)]. ^{1}H NMR (300 MHz, acetone-d_6, 298 K)/ppm: δ 3.4 (m, 6H, −CH_2−), 6.9−7.4 (m, 60H, −Ph), 7.6 (m, 6H, Ph), 7.8 (m, 4H, Ph). ^{31}P{^{1}H} NMR (202 MHz, acetone-d_6, 298 K)/ppm: δ −3.6. Positive FAB-MS: m/z 1594 [M − PF_6]$^+$. Anal. Calcd for $Cu_3C_{95}H_{76}P_7F_6{\cdot}{}^1/_2CH_2Cl_2$: C, 64.38; H, 4.36. Found: C, 64.55; H, 4.50.

$[Cu_3(\mu\text{-dppm})_3(\mu_3\text{-}\eta^1\text{-}C{\equiv}C{-}C{\equiv}C{-}C_6H_4{-}CH_3\text{-}p)_2]PF_6$ (2). This compound was prepared according to a procedure similar to that of **1** except HC≡C−C≡C−C_6H_4−CH_3-*p* (0.034 g, 0.24 mmol) was used in place of HC≡C−C≡C−Ph. Orange crystals of **2** were obtained. Yield: 0.06 g (57%). UV/vis (CH_2Cl_2), λ/nm (ϵ_{max}/dm^3 mol^{-1} cm^{-1}): 266 (80 380), 298sh (67 090), 336sh (36 200), 364sh (26 680). Raman (solid) ν/cm^{-1}: 1983s, 2162s [ν(C≡C−C≡C)]. ^{1}H NMR (300 MHz, acetone-d_6, 298 K)/ppm: δ 2.5 (s, 6H, −CH_3), 3.4 (m, 6H, −CH_2−), 7.0−7.3 (m, 60H, −Ph), 7.4 (d, 4H, J = 7.7 Hz, −C_6H_4−), 7.7 (d, 4H, J = 7.7 Hz, −C_6H_4−). ^{31}P{^{1}H} NMR (202 MHz, acetone-d_6, 298 K)/ppm: δ −3.7. Positive FAB-MS: m/z 1621 [M − PF_6]$^+$. Anal. Calcd for $Cu_3C_{97}H_{80}P_7F_6$: C, 65.93; H, 4.56. Found: C, 66.02; H, 4.47.

$[Cu_3(\mu\text{-dppm})_3(\mu_3\text{-}\eta^1\text{-}C{\equiv}C{-}C{\equiv}C{-}C_6H_4\text{-}OCH_3\text{-}p)_2]PF_6$ (3). This compound was prepared by a method similar to that of **1** except HC≡C−C≡C−C_6H_4−OCH_3-*p* (0.037 g, 0.24 mmol) was used in place of HC≡C−C≡C−Ph. Yellow crystals of **3** were obtained. Yield: 0.10 g (92%). UV/vis (CH_2Cl_2), λ/nm (ϵ_{max}/dm^3 mol^{-1} cm^{-1}): 270 (86 430), 298sh (78 210), 338sh (41 210), 366sh (28 100). Raman (solid), ν/cm^{-1}: 1977s, 2154s [ν(C≡C−C≡C)]. ^{1}H NMR (300 MHz, acetone-d_6, 298 K)/ppm: δ 3.4 (m, 6H, −CH_2−), 4.0 (s, 6H, −OCH_3), 7.0−7.3 (m, 64H, −C_6H_4− and −Ph), 7.7 (d, 4H, J = 7.8 Hz, −C_6H_4−). ^{31}P{^{1}H} NMR (202 MHz, acetone-d_6, 298 K)/ppm: δ −3.8. Positive FAB-MS: m/z 1653 [M − PF_6]$^+$. Anal. Calcd for $Cu_3C_{97}H_{80}O_2P_7F_6$: C, 64.75; H, 4.48. Found: C, 64.44; H, 4.49.

$[Cu_3(\mu\text{-dppm})_3(\mu_3\text{-}\eta^1\text{-}C{\equiv}C{-}C{\equiv}C{-}{}^nC_6H_{13})_2]PF_6$ (4). This compound was prepared by the method similar to that of **1** except HC≡C−C≡C−$^nC_6H_{13}$ (0.016 g, 0.12 mmol) was used in place of HC≡C−C≡C−Ph. Orange crystals of **4** were obtained. Yield: 0.07 g (68%). UV/vis (CH_2Cl_2), λ/nm (ϵ_{max}/dm^3 mol^{-1} cm^{-1}): 264sh (46 350), 296sh (29 090), 344sh (10 710). Raman (solid), ν/cm^{-1}: 1960s, 2188s [ν(C≡C−C≡C)]. ^{1}H NMR (300 MHz, acetone-d_6, 298 K)/ppm: δ 0.9 (t, 6H, J = 6.6 Hz, −CH_3), 1.3−1.9 (m, 16H, −$CH_2CH_2CH_2CH_2$), 2.8 (t, 4H, J = 7.7 Hz, −CH_2−C≡C), 3.4 (m, 6H, P−CH_2−P), 7.0−7.4 (m, 60H, −Ph). ^{31}P{^{1}H} NMR (202 MHz, acetone-d_6, 298 K)/ppm: δ −4.1. Positive FAB-MS: m/z 1610 [M − PF_6]$^+$. Anal. Calcd for $Cu_3C_{97}H_{80}P_7F_6{\cdot}{}^1/_2CH_2Cl_2$: C, 63.75; H, 5.12. Found: C, 64.02; H, 5.37.

$[Cu_3(\mu\text{-dppm})_3(\mu_3\text{-}\eta^1\text{-}C{\equiv}CC{\equiv}CH)_2]PF_6$ (5). A mixture of $[Cu_2(\mu\text{-dppm})_2(MeCN)_2](PF_6)_2$ (0.2 g, 0.11 mmol) and TMS−C≡C−C≡C−TMS (0.04 g, 0.21 mmol) in the presence of an excess of KF in acetone/MeOH (15 mL/5 mL) was stirred at room temperature for 24 h. After evaporation to dryness, the solid residue was extracted with CH_2Cl_2. Subsequent diffusion of diethyl ether vapor into the concentrated solution resulted in the formation of yellow crystals of **5**. Yield: 0.110 g (63%). UV/vis (CH_2Cl_2), λ/nm (ϵ_{max}/dm^3 mol^{-1} cm^{-1}): 264 (85 300), 276sh (72 530), 356sh (11 290). Raman (CH_2Cl_2), ν/cm^{-1}: 2105s [ν(C≡C−C≡C)]. ^{1}H NMR (300 MHz, acetone-d_6, 298 K)/ppm: δ 3.4 (m, 6H, −CH_2−), 3.6 (s, 2H, −C≡CH), 6.9−7.3 (m, 60H, −Ph). ^{31}P{^{1}H} NMR (202 MHz, acetone-d_6, 298 K)/ppm: δ −3.2. Positive FAB-MS: m/z 1440 [M − PF_6]$^+$. Anal. Calcd for $Cu_3C_{83}H_{68}P_7F_6$: C, 62.82; H, 4.29. Found: C, 62.87; H, 4.35.

Syntheses of Trinuclear Silver(I) Complexes. All reactions were carried out under anaerobic and anhydrous conditions using standard Schlenk techniques.

$[Ag_3(\mu\text{-dppm})_3(\mu_3\text{-}\eta^1\text{-}C{\equiv}C{-}C{\equiv}C{-}Ph)_2]PF_6$ (6). A mixture of $[Ag_2(\mu\text{-dppm})_2(MeCN)_2](PF_6)_2$ (0.12 g, 0.09 mmol) and HC≡C−C≡C−Ph (0.03 g, 0.24 mmol) in the presence of an excess of KOH in acetone/MeOH (15 mL/5 mL) was stirred at room temperature for 24 h. After evaporation to dryness, the solid residue was extracted with CH_2Cl_2. Subsequent diffusion of diethyl ether vapor into the concentrated solution resulted in the formation of colorless crystals of **6**. Yield: 0.039 g (35%). UV/vis (CH_2Cl_2), λ/nm (ϵ_{max}/dm^3 mol^{-1} cm^{-1}): 270sh (74 210), 294sh (37 670), 314 (28 550), 334 (14870). Raman (solid), ν/cm^{-1}: 2000s, 2176s [ν(C≡C−C≡C)]. ^{1}H NMR (300 MHz, acetone-d_6, 298 K)/ppm: δ 3.6 (m, 6H, −CH_2−), 7.0−7.6 (m, 60H, −Ph). ^{31}P{^{1}H} NMR (202 MHz, acetone-d_6, 298 K)/ppm: δ 2.5, 4.2.

(13) (a) Yam, V. W. W. *J. Photochem. Photobiol. A, Chem.* **1997**, *106*, 75. (b) Yam, V. W. W.; Lo, K. K. W.; Fung, W. K. M.; Wang, C. R. *Coord. Chem. Rev.* **1998**, *171*, 17. (c) Yam, V. W. W.; Fung, W. K. M.; Cheung, K. K. *J. Cluster Sci.* **1999**, *10*, 37. (d) Yam, V. W. W.; Lo, K. K. W.; Wong, K. M. T. *J. Organomet. Chem.* **1999**, *578*, 3. (e) Yam, V. W. W.; Lo, K. K. W.; Fung, W. K. M.; Wang, C. R. *Chem. Phys. Lett.* **1998**, *296*, 505.

(14) (a) Yam, V. W. W.; Lee, W. K.; Cheung, K. K. *J. Chem. Soc., Dalton Trans.* **1996**, 2335. (b) Yam, V. W. W.; Choi, S. W. K.; Chan, C. L.; Cheung, K. K. *Chem. Commun.* **1996**, 2067.

(15) Yam, V. W. W.; Lam, C. H.; Zhu, N. *Inorg. Chim. Acta* **2002**, *331*, 239.

(16) (a) Diez, J.; Gamasa, M. P.; Gimeno, J.; Tiripicchio, A.; Camellini, M. T. *J. Chem. Soc., Dalton Trans.* **1987**, 1275. (b) Lusser, M.; Peringer, P. *Polyhedron* **1985**, *4*, 1997.

(17) Eastmond, R.; Walton, D. R. M. *Tetrahedron* **1972**, *28*, 4591.

(18) Miller, J. A.; Zweifiel, G. *Synthesis* **1983**, 128.

(19) (a) Perrin, D. D.; Armarego, W. L. F.; Perrin, D. R. *Purification of Laboratory Chemicals*, 2nd ed.; Pergamon: Oxford, U.K., 1980. (b) Che, C. M.; Wong, K. Y.; Anson, F. C. *J. Electronanal. Chem. Interfacial Electrochem.* **1987**, *226*, 221.

Positive FAB-MS: m/z 1728 $[M - PF_6]^+$. Anal. Calcd for $Ag_3C_{95}H_{76}P_7F_6 \cdot {}^1/_2CH_2Cl_2$: C, 59.91; H, 4.00. Found: C, 59.62; H, 4.20.

$[Ag_3(\mu\text{-dppm})_3(\mu_3\text{-}\eta^1\text{-}C{\equiv}C{-}C{\equiv}C{-}C_6H_4{-}OCH_3\text{-}p)_2]PF_6$ (7). This compound was prepared by the method similar to that of **6** except $HC{\equiv}C{-}C{\equiv}C{-}C_6H_4{-}OCH_3$-*p* (0.037 g, 0.24 mmol) was used in place of $HC{\equiv}C{-}C{\equiv}C{-}$Ph. Colorless crystals of **7** were obtained. Yield: 0.028 g (25%). UV/vis (CH_2Cl_2), λ/nm (ϵ_{max}/dm^3 mol^{-1} cm^{-1}): 266 (72 430), 298sh (47 410), 318sh (23 970), 340 (19 080). Raman (solid), ν/cm^{-1}: 1999s, 2175s [$\nu(C{\equiv}C{-}C{\equiv}C)$]. ^{1}H NMR (300 MHz, acetone-d_6, 298 K)/ppm: δ 3.6 (m, 6H, $-CH_2-$), 3.9 (s, 6H, $-OCH_3$), 7.0−7.5 (m, 64H, $-C_6H_4-$ and −Ph), 7.6 (d, 4H, J = 8.7 Hz, Ph). ^{31}P{^{1}H} NMR (202 MHz, acetone-d_6, 298 K)/ppm: δ 2.2, 3.9. Positive FAB-MS: m/z 1403 $[M - dppm - PF_6]^+$. Anal. Calcd for $Ag_3C_{97}H_{80}O_2P_7F_6$: C, 60.3; H, 4.17. Found: C, 60.15; H, 4.15.

Physical Measurements and Instrumentation. ^{1}H and ^{31}P NMR spectra were recorded on either a Bruker AM-500 (500 MHz) or a Bruker DPX-300 (300 MHz) multinuclear FT-NMR spectrometers. Chemical shifts (δ, ppm) were reported relative to tetramethylsilane (Me_4Si) for ^{1}H and 85% H_3PO_4 for ^{31}P NMR spectroscopy. Positive ion FAB mass spectra were recorded on a Finnigan MAT95 mass spectrometer. Raman spectra were recorded as solid samples on a Bio-Rad FT-Raman spectrometer with the 1064 nm line of a Nd:YAG laser as the excitation source. Elemental analyses of the newly synthesized complexes were performed on a Carlo Erba 1106 elemental analyzer at the Institute of Chemistry, Chinese Academy of Sciences. Cyclic voltammetric measurements were performed by using a CH Instruments, Inc. model CHI 620 electrochemical analyzer interfaced to an IBM-compatible personal computer. The electrolytic cell used was a conventional two compartment cell. The salt bridge of the reference electrode was separated from the working electrode compartment by a Vycor glass. A $Ag/AgNO_3$ (0.1 M in MeCN) reference electrode was used. The ferrocenium−ferrocene couple was used as the internal standard in the electrochemical measurements in acetonitrile (0.1 M ^{n}Bu$_4$NPF$_6$). The working electrode was a glassy-carbon (Atomergic Chemetals V25) electrode with a platinum foil acting as the counter electrode. Treatment of the electrode surfaces was as reported elsewhere.[19b]

The electronic absorption spectra were obtained on a Hewlett-Packard 8452A diode array spectrophotometer. Steady-state emission spectra recorded at room temperature and at 77 K were obtained on a Spex Fluorolog-2 model 111 fluorescence spectrophotometer with or without corning filters. All solutions for photophysical studies were prepared under high-vacuum in a 10-cm^3 round-bottomed flask equipped with a sidearm 1-cm fluorescence cuvette and sealed from the atmosphere by a Rotaflo HP6/6 quick-release Teflon stopper. Solutions were rigorously degassed on a high-vacuum line in a two-compartment cell with no less than four successive freeze−pump−thaw cycles. Solid-state photophysical measurements were carried out with the solid sample loaded in a quartz tube inside a quartz-walled Dewar flask. Liquid nitrogen was placed into the Dewar flask for low temperature (77 K) solid-state photophysical measurements. Emission lifetime measurements were performed using a conventional laser system. The excitation source was the 355 nm output (third harmonic) of a Spectra-Physics Quanta-Ray Q-switched GCR-150-10 pulsed Nd:YAG laser. Luminescence decay signals were detected by a Hamamatsu R928 PMT and recorded on a Tektronix model TDS-620A (500 MHz, 2GS/s) digital oscilloscope and analyzed using a program for exponential fits. Time-resolved transient absorption spectroscopy was performed using the 355-nm output (third harmonic) of the Spectra-Physics Quanta-Ray Q-switched GCR-150-10 pulsed Nd:YAG laser as the excitation source, with the monitoring light beam generated from a 250-W quartz-tungsten-halogen lamp placed perpendicular to the excitation beam. The output of the quartz-tungsten-halogen lamp was wavelength selected by passing through two monochromators (Oriel 77250, $^1/_8$ m and 77 200, $^1/_4$ m). The transient absorption signals were detected by a Hamamatsu R928 photomultiplier tube connected to a 50-Ω resistor and amplified by a Tektronix AM 502 differential amplifier (<1 MHz) and digitized on a Tektronix model TDS-620A (500 MHz, 2GS/s) digital oscilloscope interfaced to an IBM-compatible personal computer for data acquisition and analysis. The transient absorption difference spectra were generated using the point-to-point method. The back-electron-transfer (BET) rate constants (k_{bet}) was obtained from a knowledge of the slope (m) of a plot of the reciprocal of absorbance change either at 400 nm or at 790−810 nm ($1/\Delta A$) versus time (t) for the transient signal with $k_{bet} = (\Delta\epsilon)bm$ where $\Delta\epsilon$ is the extinction coefficient difference between products and reactants at the monitored wavelength and b is the path length of the cell. The plot is linear over at least 2.5 half-lives, indicative of second-order kinetics.

Crystal Structure Determination. Single crystals of $[Cu_3(\mu\text{-dppm})_3(\mu_3\text{-}\eta^1\text{-}C{\equiv}CC{\equiv}CPh)_2]PF_6$ (**1**) and $[Cu_3(\mu\text{-dppm})_3(\mu_3\text{-}\eta^1\text{-}C{\equiv}CC{\equiv}CH)_2]PF_6$ (**5**) suitable for X-ray diffraction studies were grown by layering of *n*-hexane onto a concentrated acetone solution of the complex. Crystal structure determination data as well as the selected bond distances and bond angles for complex **1** and **5** are summarized in Table 1 and 2, respectively. The X-ray diffraction data were collected at 28 °C on a MAR diffractometer with a 300 mm image plate detector using graphite monochromatized Mo Kα radiation (λ = 0.710 73 Å). The images were interpreted and intensities integrated using program *DENZO*.[20a] The structure was solved by direct methods employing the SIR-97 program.[20b] Full-matrix least-squares refinement on F^2 was used in the structure refinement. The positions of H atoms are calculated based on riding mode with thermal parameters equal to 1.2 times that of the associated C atoms and participated in the calculation of final R-indices.[21] In the final stage of least-squares refinement, all non-hydrogen atoms were refined anisotropically. One crystallographic asymmetric unit consists of one formula unit for **1**, including two PF_6^- anions and one Et_3NH^+ cation. One crystallographic asymmetric unit consists of one formula unit for **5**.

Theoretical Calculations. A. Density Funtional Theory Calculations. Density functional theory (DFT) calculations were carried out on model compounds derived from the experimental structure data using the Amsterdam Density Functional (ADF) program[22] developed by Baerends and co-workers[23] using the local density approximation (LDA) in the Vosko−Wilk−Nusair parametrization[24] and the nonlocal corrections for exchange and correlation of Becke[25] and Perdew,[26] respectively. The atom electronic configurations were described by a triple-ζ Slater-type orbital (STO) basis set for H 1s, C 2s and 2p, P 3s and 3p augmented with a 3d single-ζ polarization for C and P atoms and with a 2p single-ζ polarization for H atoms. A triple-ζ STO basis set was used for Cu 3d and 4s, augmented with a single-ζ 4p polarization function for Cu. A frozen-core approximation was used to treat the core shells up to 1s for C, 2p for P, and 3p for Cu.[23] Geometries were optimized using the analytical gradient method

(20) (a) Otwinowski, Z.; Minor, W. Processing of X-ray Diffraction Data Collected in Oscillation Mode. In *Methods in Enzymology, Volume 276: Macromolecular Crystallography, part A*; Charles, C. W., Sweet, R. M., Jr., Eds.; Academic Press: San Diego, 1997; pp 307−326. (b) Sheldrick, G. M. *SHELX97, Programs for Crystal Structure Analysis*, release 97-2; University of Göttingen: Germany, 1997.

(21) Since the structure refinements are against F^2, R-indices based on F^2 are larger than (more than double) those based on F. For comparison with older refinements based on F and an OMIT threshold, a conventional index R_1 based on observed F values larger than $4\sigma(F_o)$ is also given (corresponding to intensity (I) ≥ $2\sigma(I)$). $wR_2 = \{[w(F_o^2 - F_c^2)^2]/[w(F_o^2)^2]\}^{1/2}$, $R_1 = ||F_o| - |F_c||/|F_o|$. The goodness of fit (GooF) is always based on F^2: GooF = $S = \{[w(F_o^2 - F_c^2)^2]/(n - p)\}^{1/2}$, where n is the number of reflections and p is the total number of parameters refined. The weighting scheme is: $w = 1/[\sigma^2(F_o^2) + (aP)^2 + bP]$, where P is $[2F_c^2 + \mathrm{Max}(F_o^2, 0)]/3$.

(22) *ADF2.3* and *ADF2002.01*; SCM: Theoretical Chemistry, Vrije Universiteit, Amsterdam, The Netherlands, http://www.scm.com.

(23) (a) te Velde, G.; Bickelhaupt, F. M.; van Gisbergen, S. J. A.; Fonseca Guerra, C.; Baerends, E. J.; Snijders, J. G.; Ziegler, T. J. *Comput. Chem.* **2001**, *22*, 931. (b) Fonseca Guerra, C.; Snijders, J. G.; te Velde, G.; Baerends, E. J. *Theor. Chem. Acc.* **1998**, *99*, 391.

(24) Vosko, S. D.; Wilk, L.; Nusair, M. *Can. J. Chem.* **1990**, *58*, 1200.

(25) (a)Becke, A. D. *J. Chem. Phys.* **1986**, *84*, 4524. (b) Becke, A. D. *Phys. Rev. A.* **1988**, *38*, 3098.

(26) Perdew, J. P. *Phys. Rev. B* **1986**, *33*, 8822; *34*, 7406.

Table 1. Crystal and Structure Determination Data of **1** and **5**

complex	**1**	**5**
empirical formula	$C_{101}H_{92}Cu_3F_{12}NP_8$	$C_{83}H_{68}Cu_3F_6P_7$
formula weight	1986.14	1586.78
temperature	301 K	301 K
wavelength	0.710 73 Å	0.710 73 Å
crystal system	monoclinic	monoclinic
space group	$P2_1/c$	$P2_1/n$
A	24.089(3) Å	14.633(2) Å
B	14.957(3) Å	27.457(4) Å
C	28.235(3) Å	19.035(3) Å
α	90°	90°
β	110.53(3)°	106.80(3)°
γ	90°	90°
volume	9527(3) Å^3	7321.4(19) Å^3
Z	4	4
F(000)	4080	3248
density (calculated)	1.385 mg m^{-3}	1.440 mg m^{-3}
crystal size	0.35 × 0.25 × 0.05 mm^3	0.4 × 0.25 × 0.2 mm^3
collection range	$2\theta_{max} = 48.8°$	$2\theta_{max} = 51.04°$
index ranges	$0 \le h \le 27, 0 \le k \le 16, -31 \le l \le 29$	$-17 \le h \le 17, -3 \le k \le 33, -22 \le l \le 22$
reflections collection	11 937	41 952
goodness-of-fit on F^2	0.963	1.009
final *R* indices[a]	$[I > 2\sigma(I)]$ $R_1 = 0.0576$, $wR = 0.1500$	$[I > 2\sigma(I)]$ $R_1 = 0.0527$, $wR_2 = 0.1437$
largest diff. peak and hole	+0.474 and −0.762 e·Å^{-3}	+0.639 and −0.761 e·Å^{-3}

[a] $R_{int} = \sum|F_o^2 - F_o^2(\text{mean})|/\sum[F_o^2]$, $R_1 = \sum||F_o| - |F_c||/\sum|F_o|$ and $wR_2 = \{\sum[w(F_o^2 - F_c^2)^2]/\sum[w(F_o^2)^2]\}^{1/2}$.

implemented by Verluis and Ziegler.[27] Electronic absorption spectra were predicted using the time-dependent density functional theory (TD-DFT) method implemented within the ADF program using the default optimization criteria.[28] The representations of the molecular orbitals were done using MOLEKEL4.1.[29]

B. Extended Hückel Calculations. Extended Hückel (EH) calculations were carried out within the extended Hückel formalism[30] using the CACAO program.[31] The Slater exponents (*ζ*) and the valence shell ionization potentials (H_{ii} in eV) were respectively: 1.3, −13.6 for H 1s; 1.625, −21.4 for C 2s; 1.625, −11.4 for C 2p; 1.600, −18.6 for P 3s; 1.600, −14.0 for P 3p; 2.200, −11.40 for Cu 4s; 2.200, −6.06 for Cu 4p. The H_{ii} value for Cu 3d was at −14.00. A linear combination of two Slater-type orbitals with exponents $\zeta_1 = 5.95$ and $\zeta_2 = 2.30$ with the weighting coefficients $c_1 = 0.5933$ and $c_2 = 0.5744$ were used to represent the Cu 3d atomic orbitals. EH calculations were carried out on models derived from the averaged DF-optimized geometries of $[Cu_3(\mu\text{-dHpm})_3(\mu_3\text{-}\eta^1\text{-C}{\equiv}\text{C}{-}\text{C}{\equiv}\text{CH})_2]^+$ (**5-H**) and $[Cu_3(\mu\text{-dHpm})_3(\mu_3\text{-}\eta^1\text{-C}{\equiv}\text{CH})_2]^+$ (**8-H**).

Results and Discussion

Synthesis. Trinuclear bi-capped copper(I) diynyl complexes, $[Cu_3(\mu\text{-dppm})_3(\mu_3\text{-}\eta^1\text{-C}{\equiv}\text{C}{-}\text{C}{\equiv}\text{C}{-}\text{R})_2]PF_6$ [R = Ph (**1**), C_6H_4—CH_3-*p* (**2**), C_6H_4—OCH_3-*p* (**3**), $^nC_6H_{13}$ (**4**)] were prepared by treatment of $[Cu_2(\mu\text{-dppm})_2(MeCN)_2](PF_6)_2$ with the corresponding diyne in a molar ratio of 3:8 with a 1-fold excess of diyne in the presence of an excess of KOH in acetone/MeOH (3:1 v/v) mixture. Alternatively, use of triethylamine instead of KOH as the base to deprotonate the diyne also gave the desired products but in lower yield. Butadiynyl copper(I) complexes, $[Cu_3(\mu\text{-dppm})_3(\mu_3\text{-}\eta^1\text{-C}{\equiv}\text{C}{-}\text{C}{\equiv}\text{CH})_2]PF_6$ (**5**), were prepared by the reaction between 1,4-bis(trimethylsilyl)-1,3-butadiyne and $[Cu_2(\mu\text{-dppm})_2(MeCN)_2](PF_6)_2$ in a 3:8 ratio in the presence of KF in acetone/MeOH (3:1 v/v) mixture. Trinuclear bicapped silver(I) diynyl complexes, $[Ag_3(\mu\text{-dppm})_3(\mu_3\text{-}\eta^1\text{-C}{\equiv}\text{C}{-}\text{C}{\equiv}\text{C}{-}\text{R})_2]PF_6$ [R = Ph (**6**), C_6H_4—OCH_3-*p* (**7**)], were obtained by a method similar to that for the preparation of the bicapped copper(I) diynyl complexes except $[Ag_2(\mu\text{-dppm})_2(MeCN)_2](PF_6)_2$ was used in place of $[Cu_2(\mu\text{-dppm})_2(MeCN)_2](PF_6)_2$. All the newly synthesized copper(I) and silver(I) complexes gave satisfactory elemental analyses and were characterized by positive FAB-MS, Raman, ^{1}H, and ^{31}P NMR spectroscopy.

The FT-Raman spectra of the trinuclear copper(I) diynyl complexes revealed two strong bands at ca. 1980 and 2160 cm^{-1}, characteristic of the ν(C≡C) stretches of the diynyl ligand. Similar bands were too weak to be observed in the IR spectra. Similarly, the ν(C≡C) stretches of the silver(I) diynyl complexes were observed at ca. 2000 and 2175 cm^{-1}. The $^{31}P\{^1H\}$ spectra for the trinuclear copper(I) diynyl complexes exhibit a singlet at ca. δ −3.2 to −4.1 showing that the six phosphorus atoms are chemically equivalent. The upfield ^{31}P NMR chemical shift observed from δ −3.2 to −4.1 upon going from **5** to **1** to **2** to **3** to **4** are in line with the increasing electron richness of the diynyl ligands in the order: **5** < **1** < **2** ≤ **3** < **4**. The $^{31}P\{^1H\}$ spectra for the trinuclear silver(I) diynyl complexes showed two unresolved signals at ca. δ 2.2−2.5 and 3.9−4.2 arising from ^{107}Ag−^{31}P and ^{109}Ag−^{31}P spin−spin coupling.

Crystal Structure Determination. The perspective drawings of the complex cations of $[Cu_3(\mu\text{-dppm})_3(\mu_3\text{-}\eta^1\text{-C}{\equiv}\text{CC}{\equiv}\text{CPh})_2]PF_6$ (**1**) and $[Cu_3(\mu\text{-dppm})_3(\mu_3\text{-}\eta^1\text{-C}{\equiv}\text{CC}{\equiv}\text{CH})_2]PF_6$ (**5**) are depicted in Figures 1 and 2, respectively.

Both complex cations consist of an isosceles triangle of copper atoms with a dppm ligand bridging each edge to form a roughly planar $[Cu_3P_6]$ core. The Cu_2P_2C rings adopt envelope conformations with the methylene carbon atoms on the flap, one of them folded toward one of the faces of the triangle and the other two folded away from it. In the complex, each diynyl ligand is C-bonded to the three copper atoms, showing an asymmetric μ_3-η^1 bridging mode with the copper-to-carbon distances significantly different. The Cu−C bond distances in **1** and **5** are in the range of 2.02(2)−2.49(4) Å and 2.084(6)−

(27) Verluis, L.; Ziegler, T. *J. Chem. Phys.* **1988**, *88*, 322.
(28) van Gisbergen, S. J. A.; Snijders, J. G.; Baerends, E. J. *Comput. Phys. Commun.* **1999**, *118*, 119.
(29) Flükiger, P.; Lüthi, H. P.; Portmann, S.; Weber, J. *Molekel 4.1*; Swiss Center for Scientific Computing (CSCS): Manno, Switzerland, 2000−2001.
(30) Hoffmann, R. *J. Chem. Phys.* **1963**, *39*, 1397.
(31) Mealli, C.; Proserpio, D. *J. Chem. Educ.* **1990**, *67*, 399.

Table 2. Selected Bond Lengths (Å) and Angles (deg) for $[Cu_3(\mu\text{-dppm})_3(\mu_3\text{-}\eta^1\text{-}C{\equiv}CC{\equiv}CPh)_2]PF_6$ (**1**) and for $[Cu_3(\mu\text{-dppm})_3(\mu_3\text{-}\eta^1\text{-}C{\equiv}CC{\equiv}CH)_2]PF_6$ (**5**), with Estimated Standard Deviations (esd's) Given in Parentheses

$[Cu_3(\mu\text{-dppm})_3(\mu_3\text{-}\eta^1\text{-}C{\equiv}CC{\equiv}CPh)_2]PF_6$ (**1**)

Bond Lengths (Å)			
Cu(1)···Cu(2)	2.602(2)	C(3)−C(4)	1.24(3)
Cu(2)···Cu(3)	2.619(2)	C(11)−Cu(1)	2.43(9)
Cu(1)···Cu(3)	2.742(2)	C(11)−Cu(2)	2.19(2)
C(1)−Cu(1)	2.02(2)	C(11)−Cu(3)	2.04(2)
C(1)−Cu(2)	2.11(2)	C(11)−C(12)	1.24(2)
C(1)−Cu(3)	2.49(4)	C(12)−C(13)	1.34(3)
C(1)−C(2)	1.20(2)	C(13)−C(14)	1.15(2)
C(2)−C(3)	1.45(3)		
Bond Angles (deg)			
Cu(1)−Cu(2)−Cu(3)	63.35(5)	C(2)−C(3)−C(4)	177(1)
Cu(1)−Cu(3)−Cu(2)	58.02(5)	Cu(1)−C(11)−Cu(3)	74.9(5)
Cu(2)−Cu(1)−Cu(3)	58.62(5)	Cu(2)−C(11)−Cu(3)	76.3(6)
Cu(1)−C(1)−Cu(2)	78.2(6)	Cu(1)−C(11)−Cu(2)	68.0(1)
Cu(1)−C(1)−Cu(3)	73.9(4)	Cu(1)−C(11)−C(12)	110.2(7)
Cu(2)−C(1)−Cu(3)	68.7(4)	Cu(2)−C(11)−C(12)	129.7(9)
Cu(1)−C(1)−C(2)	146(1)	Cu(3)−C(11)−C(12)	153.9(1)
Cu(2)−C(1)−C(2)	131(1)	C(11)−C(12)−C(13)	173(1)
Cu(3)−C(1)−C(2)	126(9)	C(12)−C(13)−C(14)	174(1)
C(1)−C(2)−C(3)	178(1)		

$Cu_3(\mu\text{-dppm})_3(\mu_3\text{-}\eta^1\text{-}C{\equiv}CC{\equiv}CH)_2]PF_6$ (**5**)

Bond Lengths (Å)			
Cu(1)···Cu(2)	2.7755(9)	C(3)−C(4)	1.185(8)
Cu(2)···Cu(3)	2.8624(8)	C(5)−Cu(1)	2.218(5)
Cu(1)···Cu(3)	2.5698(8)	C(5)−Cu(2)	2.496(6)
C(1)−Cu(1)	2.084(6)	C(5)−Cu(3)	2.089(5)
C(1)−Cu(2)	2.270(4)	C(5)−C(6)	1.149(7)
C(1)−Cu(3)	2.390(5)	C(6)−C(7)	1.377(8)
C(1)−C(2)	1.124(7)	C(7)−C(8)	1.215(9)
C(2)−C(3)	1.413(8)		
Bond Angles (deg)			
Cu(1)−Cu(2)−Cu(3)	54.21(2)	C(2)−C(3)−C(4)	177.5(6)
Cu(1)−Cu(3)−Cu(2)	61.17(2)	Cu(1)−C(5)−Cu(3)	73.18(17)
Cu(2)−Cu(1)−Cu(3)	64.62(2)	Cu(2)−C(15)−Cu(3)	76.69(18)
Cu(1)−C(1)−Cu(2)	79.09(18)	Cu(1)−C(5)−Cu(2)	71.87(16)
Cu(1)−C(1)−Cu(3)	69.74(17)	Cu(1)−C(5)−C(6)	136.4(4)
Cu(2)−C(1)−Cu(3)	75.76(15)	Cu(2)−C(5)−C(6)	115.5(4)
Cu(1)−C(1)−C(2)	175.0(5)	Cu(3)−C(5)−C(6)	149.4(4)
Cu(2)−C(1)−C(2)	101.5(4)	C(5)−C(6)−C(7)	178.3(6)
Cu(3)−C(1)−C(2)	115.3(4)	C(6)−C(7)−C(8)	177.0(9)
C(1)−C(2)−C(3)	174.0(6)		

2.496(6) Å, respectively. The bond angles between the diynyl group and each of the copper atoms in **1** and **5** are in the range of 110.2(7)°−153.9(1)° and 101.5(4)°−175.0(5)°, respectively. It is noted that one of the three Cu−C distances is relatively longer than the other two Cu−C distances. The C≡C bond distances in both complexes are in the range of 1.15(2)−1.24(3) Å and 1.149(7)−1.24(7) Å for **1** and **5**, respectively, which are characteristic of metal−alkynyl σ-bonding.[32] This is suggestive of a σ-bonding mode with the $Cu_3(\mu_3\text{-}C)_2$ core of the $[Cu_3(C{\equiv}CC{\equiv}CR)_2]$ moiety mainly described as a "5-center-4-electron" system with relatively little contribution of a π-donation from the C≡C unit (vide supra). The Cu···Cu distances in **1** and **5** are in the range of 2.602(2)−2.742(2) Å and 2.5698(8)−2.8624(8) Å, respectively. The observation of Cu···Cu distances shorter than the sum of van der Waals radii for copper (2.8 Å)[33a] may be suggestive of the presence of some weak metal−metal interactions. Such short Cu···Cu distances are also commonly observed in electron-deficient organocopper systems.[33b,c]

Bonding and Electronic Structure Calculations. To provide better insight into the electronic structures of the title compounds, in particular to explain their experimental spectroscopic, structural, and electrochemical properties, quantum chemical calculations of DFT type were first carried out using the ADF suite of programs on the hydrogen-substituted model complexes, $[Cu_3(\mu\text{-dHpm})_3(\mu_3\text{-}\eta^1\text{-}C{\equiv}C{-}C{\equiv}CH)_2]^+$ (**5-H**) and $[Cu_3(\mu\text{-dHpm})_3(\mu_3\text{-}\eta^1\text{-}C{\equiv}C{-}C{\equiv}CPh)_2]^+$ (**1-H**) of C_1 symmetry. Their electronic structure was compared and contrasted to that of the monoynyl parent molecules $[Cu_3(\mu\text{-dHpm})_3(\mu_3\text{-}\eta^1\text{-}C{\equiv}CH)_2]^+$ (**8-H**) and the hydrogen-substituted model of $[Cu_3(\mu\text{-dppm})_3(\mu_3\text{-}\eta^1\text{-}C{\equiv}C{-}CPh)_2]^+$ reported previously,[12a] $[Cu_3(\mu\text{-dHpm})_3(\mu_3\text{-}\eta^1\text{-}C{\equiv}CPh)_2]^+$ (**9-H**). Computational details are given in the Experimental Section.

As shown in Table 3, models **5-H** and **1-H** quite satisfactorily mimic the metric distances of the crystallographically characterized complexes **5** and **1**, respectively, although the computed Cu−Cu and Cu−C distances somewhat differ from the corre-

(32) Nast, R. *Coord. Chem. Rev.* **1982**, *47*, 89.
(33) (a) Slater, J. C. *J. Chem. Phys.* **1964**, *41*, 3199. (b) van Koten, G.; James, S. L.; Jastrzebski, J. T. B. H. In *Comprehensive Organometallic Chemistry II*; Abel, E. W., Stone, F. G. A., Wilkinson, G., Eds.; Pergamon: Oxford, 1995; Vol. 3, pp 57−133. (c) Hathaway, B. J. In *Comprehensive Coordination Chemistry*; Wilkinson, G., Gillard, R. D., McCleverty, J. A., Eds.; Pergamon: Oxford, 1987; Vol. 5, pp 533−774.

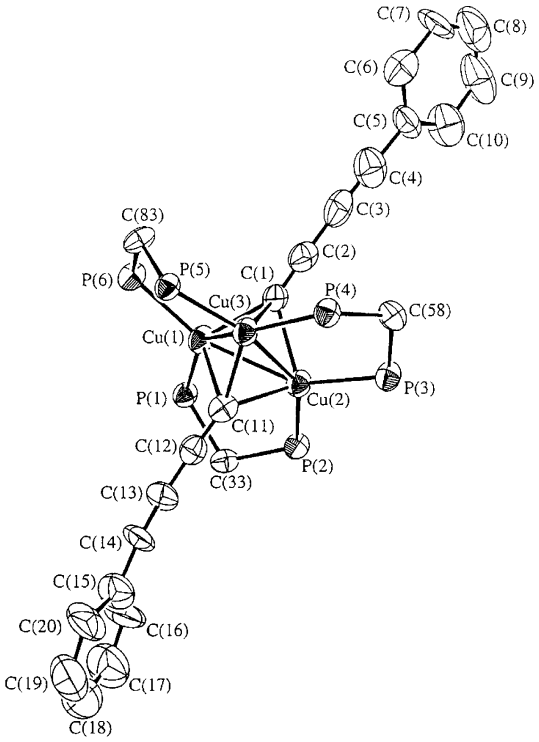

Figure 1. Perspective drawing of the complex cation of $[Cu_3(\mu\text{-dppm})_3(\mu_3\text{-}\eta^1\text{-}C{\equiv}CC{\equiv}CPh)_2]PF_6$ (**1**) with the atomic numbering scheme. Hydrogen atoms and phenyl rings of dppm ligands have been omitted for clarity. Thermal ellipsoids are shown at the 40% probability level.

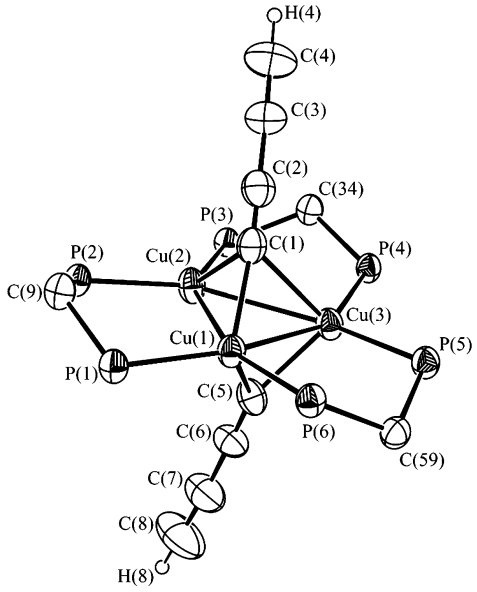

Figure 2. Perspective drawing of the complex cation of $[Cu_3(\mu\text{-dppm})_3(\mu_3\text{-}\eta^1\text{-}C{\equiv}CC{\equiv}CH)_2]PF_6$ (**5**) with the atomic numbering scheme. Hydrogen atoms and phenyl rings of dppm ligands have been omitted for clarity. Thermal ellipsoids are shown at the 40% probability level.

sponding experimental values. The Cu−C and C−C distances computed for the monoynyl analogue model **9-H** essentially reproduce the experimental structure of compound **9**,[34] giving confidence in the computed bond lengths in model **8-H** for which no X-ray data are available yet. The distance values are quite similar to those in models **5-H** and **1-H** with two rather short and one rather long Cu−C distances (see Table 3).

(34) Diéz, J.; Gamasa, M. P.; Gimeno. J.; Aguirre, A.; García-Granda, S. *Organometallics* **1991**, *10*, 380.

Table 3. Pertinent DFT Results: HOMO−LUMO Gap (eV), Selected Computed Bond Lengths (Å), and Hirshfeld Atomic Charges for the Model Complexes $[Cu_3(\mu\text{-dHpm})_3(\mu_3\text{-}\eta^1\text{-}C{\equiv}C{-}C{\equiv}CH)_2]^+$ (**5-H**), $[Cu_3(\mu\text{-dHpm})_3(\mu_3\text{-}\eta^1\text{-}C{\equiv}CH)_2]^+$ (**8-H**), $[Cu_3(\mu\text{-dHpm})_3(\mu_3\text{-}\eta^1\text{-}C{\equiv}C{-}C{\equiv}CPh)_2]^+$ (**1-H**), and $[Cu_3(\mu\text{-dHpm})_3(\mu_3\text{-}\eta^1\text{-}C{\equiv}CPh)_2]^+$ (**9-H**), with Experimental Bond Lengths (Å) Given in Parentheses for $[Cu_3(\mu\text{-dppm})_3(\mu_3\text{-}\eta^1\text{-}C{\equiv}C{-}C{\equiv}CH)_2]^+$ (**5**), $[Cu_3(\mu\text{-dppm})_3(\mu_3\text{-}\eta^1\text{-}C{\equiv}C{-}C{\equiv}CPh)_2]^+$ (**1**), and $[Cu_3(\mu\text{-dppm})_3(\mu_3\text{-}\eta^1\text{-}C{\equiv}CPh)_2]^+$ (**9**) for Comparison

complex	5-H	8-H	1-H	9-H
		HOMO−LUMO Gap		
	3.08	3.40	2.60	2.98
		Bond Lengths		
Cu(1)−Cu(2)	2.736(2.8624)	2.712	2.742(2.742)	2.662(2.603)
Cu(2)−Cu(3)	2.713(2.7755)	2.663	2.668(2.619)	2.656(2.584)
Cu(1)−Cu(3)	2.662(2.5698)	2.643	2.653(2.602)	2.623(2.565)
Cu(1)−C(α)	2.292(2.390)	2.352	2.457(2.43)	2.333(2.331)
Cu(2)−C(α)	2.152(2.270)	2.241	2.239(2.19)	2.157(2.154)
Cu(3)−C(α)	2.070(2.084)	2.067	2.015(2.04)	2.127(2.115)
Cu(1)−C(α′)	2.020(2.089)	2.104	2.037(2.02)	2.085(2.061)
Cu(2)−C(α′)	2.352(2.218)	2.156	2.156(2.11)	2.229(2.186)
Cu(3)−C(α′)	2.424(2.496)	2.432	2.454(2.49)	2.340(2.323)
C(α)−C(β)	1.249(1.124)	1.234	1.251(1.24)	1.243(1.234)
C(β)−C(γ)	1.357(1.377)		1.352(1.45)	
C(γ)−C(δ)	1.222(1.185)		1.231(1.15)	
C(α′)−C(β′)	1.248(1.149)	1.235	1.253(1.20)	1.245(1.231)
C(β′)−C(γ′)	1.364(1.413)		1.352(1.34)	
C(γ′)−C(δ′)	1.223(1.215)		1.233(1.24)	
		Hirshfeld Charges		
Cu(1)	0.19	0.18	0.16	0.16
Cu(2)	0.16	0.18	0.17	0.17
Cu(3)	0.18	0.17	0.17	0.17
C(α)	−0.26	−0.26	−0.26	−0.28
C(β)	−0.05	−0.12	−0.07	−0.06
C(γ)	−0.04		−0.05	
C(δ)	−0.06		−0.01	
C(α′)	−0.25	−0.27	−0.27	−0.28
C(β′)	−0.07	−0.12	−0.07	−0.06
C(γ′)	−0.04		−0.06	
C(δ′)	−0.08		−0.01	

It is worth mentioning that optimization of the models **5-H** and **8-H** with higher symmetry (C_s) gives geometries nearly isoenergetic to those of C_1 symmetry, though the Cu−Cu and Cu−C distances somewhat differ. This reflects indeed the "soft" bonding interaction between the d^{10} metal centers in these systems which results from a mixing of the s, p, and d levels.[35]

Calculations of extended Hückel theory (EHT) type were carried out as well on models **5-H** and **8-H** of C_s symmetry derived from the DFT-optimized structures, to analyze qualitatively the bonding between the copper triangle and the carbon moieties in this kind of cluster complex. Their EH-molecular orbital diagrams are compared in Figure 3. They were built up from the interaction of the frontier molecular orbitals (FMO) of the metallic fragment $[Cu_3(\mu\text{-dHpm})_3]^{3+}$ with those of the bis-diynyl $[(C_4H)_2]^{2-}$ or the bis-monoynyl $[(C_2H)_2]^{2-}$ ligands (the charges of the fragments are arbitrary). The metallic fragment consists of three nonconical C_{2v} d^{10} ML_2 units,[36] the FMO of which combine to yield a nest of 12 low-lying d-based MOs below a set of 9 sp and p energy-spread MOs (see the middle of Figure 3). The FMOs of the bis-diynyl $[(C_4H)_2]^{2-}$

(35) (a) Mehrotra, P. K.; Hoffmann, R. *Inorg. Chem.* **1978**, *17*, 2187. (b) Merz, K. M.; Hoffmann, R. *Inorg. Chem.* **1988**, *27*, 2120. (c) Vega, A.; Calvo, V.; Spodine, E.; Zarate, A.; Fuenzalida, V.; Saillard, J.-Y. *Inorg. Chem.* **2003**, *41*, 3389.

(36) Albright, T. A.; Burdett, J. K.; Whangbo, M.-H. *Orbital Interactions in Chemistry*; John Wiley: New York, 1985.

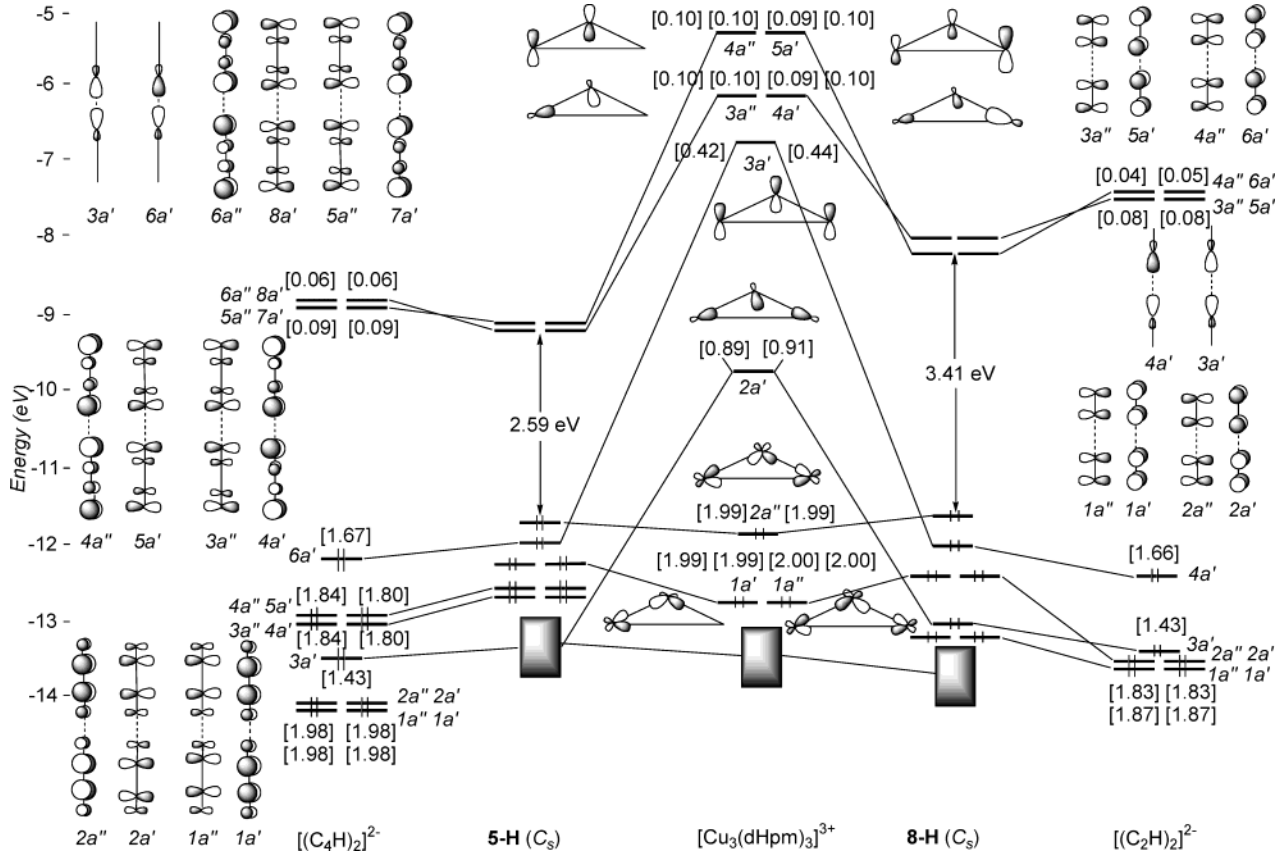

Figure 3. EH orbital interaction diagram for $[Cu_3(\mu\text{-dHpm})_3(\mu_3\text{-}\eta^1\text{-C}{\equiv}\text{CC}{\equiv}\text{CH})_2]^+$ (**5-H**) (left) and $[Cu_3(\mu\text{-dHpm})_3(\mu_3\text{-}\eta^1\text{-C}{\equiv}\text{CH})_2]^+$ (**8-H**) (right). FMO occupations after interaction are given in brackets.

and the bis-monoynyl $[(C_2H)_2]^{2-}$ fragments consist of a set of in-phase and out-of-phase combinations of σ, π, and π^* carbon orbitals (see the left-hand and right-hand sides of Figure 3).

In both complexes, **5-H** and **8-H**, the Cu−C bonding is dominated by strong σ-type interactions between vacant metal orbitals and in-phase and out-of-phase combinations of C_4H and C_2H σ-type FMOs (see Figure 3). This leads to an important electron donation from the bis-diynyl $[(C_4H)_2]^{2-}$ and the bis-monoynyl $[(C_2H)_2]^{2-}$ fragments toward the metallic fragment as illustrated numerically by values in brackets in Figure 3 which indicate the electron occupation of FMOs after interaction of the component fragments. The strongly bonding interactions are hardly complemented by back-donation from the low-lying occupied metallic MOs into accepting π^* FMOs of the carbon units (see Figure 3). Note that the weak back-donation is very slightly more important in **5-H** than in **8-H**. Indeed, a highly delocalized 4-electron/5-center picture accounts for the Cu−C bonding in these kinds of complexes. Large HOMO−LUMO gaps are computed for both complexes **5-H** and **8-H** for the count of 46 metal valence electrons.

These qualitative conclusions are further supported by density functional molecular orbital calculations, which were carried out on **5-H** and **8-H**. Comparable Cu−C bonding reflects in the DFT computed Hirshfeld[37] atomic net charges which indicate some flow of electron density from the copper triangle to the carbon chains. It follows that a substantial amount of negative charge ends up on C(α) and to a lesser extent on the rest of the carbon ligand (see Table 3). As discussed above, this is mainly due to σ-type Cu−C interactions.

(37) $R_{int} = \Sigma|F_o^2 - F_o^2(\text{mean})|/\Sigma[F_o^2]$.

Representations for some DFT MOs in their HOMO−LUMO region are shown in Figure 4. For **5-H**, a set of four nearly degenerate MOs constitutes the HOMO region. Two of them, the HOMO and HOMO − 2 are predominantly localized on the carbon C_4 chain and to a lesser extent on the copper, whereas the HOMO − 1 and HOMO − 3 are heavily weighed on the copper triangle. These four occupied MOs are separated by a large gap of 3.08 eV from two nearly degenerate LUMOs strongly formed by π-type carbon orbitals with contributing copper orbitals. Variation of the carbon ligand, i.e., bis-diynyl vs bis-monoynyl, hardly affects the energy and the composition of the HOMOs. Indeed, four nearly degenerate MOs are found in the HOMO region for **8-H** as well (see Figure 4). The HOMO and HOMO − 1 are principally copper in character, whereas the HOMO − 2 and HOMO − 3 are both delocalized on the bis-monoynyl and the metal atoms. The energy and composition of the LUMOs of **8-H** are more affected. Their energy is higher than that of the LUMOs of the bis-diynyl complex, leading to a larger DFT HOMO−LUMO gap for the former (3.40 eV vs 3.08 eV). It turns out that the LUMOs are rather dHpm in character and are less heavily weighed on the carbon fragment and the metal triangle (see Figure 4). Vacant MOs strongly localized on the bis-monoynyl ligand are found higher in energy.

Comparable energy and composition of the HOMOs of the bis-diynyl-copper and the bis-monoynyl-copper complexes should lead to comparable ionization potentials (IP). This is confirmed by the vertical first ionization potentials (IP) computed for **5-H** and **8-H**. Close values are calculated (9.84 and 9.95 eV, respectively). Solution-phase oxidation potentials generally track gas-phase IPs. Indeed, fairly similar first

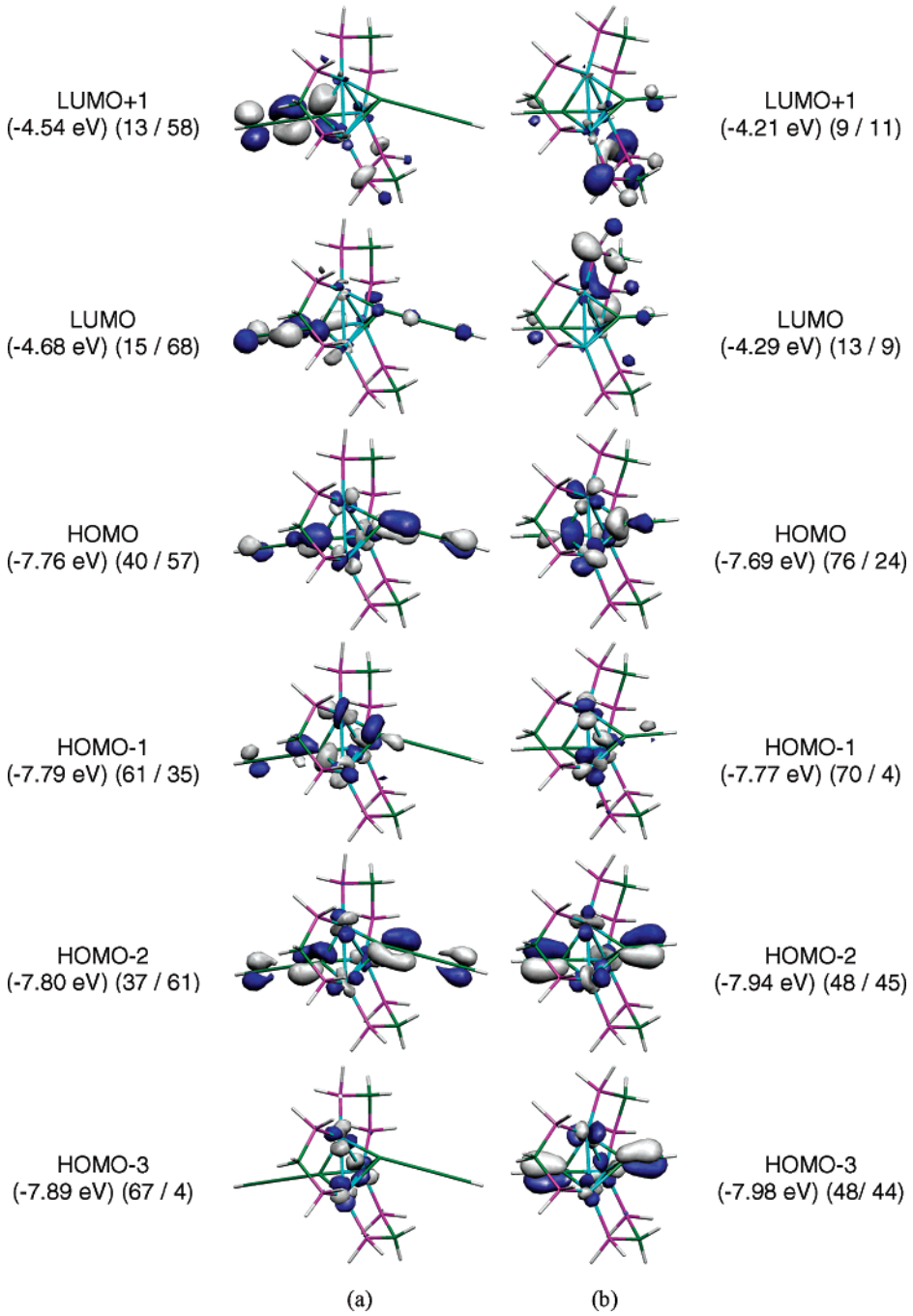

Figure 4. DFT molecular orbital plots for some frontier molecular orbitals of (a) $[Cu_3(\mu\text{-dHpm})_3(\mu_3\text{-}\eta^1\text{-C}{\equiv}\text{CC}{\equiv}\text{CH})_2]^+$ (**5-H**) and (b) $[Cu_3(\mu\text{-dHpm})_3(\mu_3\text{-}\eta^1\text{-C}{\equiv}\text{CH})_2]^+$ (**8-H**). Energy and metal (left)/carbon ligand (right) percentage contributions of the MOs are given in parentheses.

oxidation potentials are experimentally measured for complexes containing the same end group, with the monoynyl complexes only very slightly easier to oxidize than their diynyl counterparts (vide infra). On the other hand, enhancement of the electron-releasing properties of the end-group linked to the C_4 or C_2 ligands gives lower IPs. Calculations on different diynyl complex models $[Cu_3(\mu\text{-dHpm})_3(\mu_3\text{-}\eta^1\text{-C}{\equiv}\text{C}{-}\text{C}{\equiv}\text{CR})_2]^+$ (R = Ph (**1-H**), $C_6H_4{-}CH_3$-*p* (**2-H**) and $C_6H_4{-}OCH_3$-*p* (**3-H**)) indicate some significant shift to higher energy of the HOMOs. Accordingly, these compounds are more readily ionized than the hydrogenated counterpart **5-H** (e.g., 8.71 for **1-H**, 8.62 for **2-H**, and 8.58 eV for **3-H**, respectively, vs. 9.84 eV for **5-H**). This is in accordance with the electrochemical properties reported for the $[Cu_3(\mu\text{-dppm})_3(\mu_3\text{-}\eta^1\text{-C}{\equiv}\text{C}{-}\text{C}{\equiv}\text{CR})_2]^+$ series (vide infra).

Time-dependent density functional theory (TD-DFT) was used to calculate the vertical electronic transition energies of the bis-diynyl complex model **5-H** in order to gain more insight into the nature of the electronic spectral features observed for **5** and congeners. Because of the lack of symmetry of **5-H**, numerous transitions are allowed. Nevertheless, relevant to the experimental absorption spectrum of **5** which shows an absorption band at 356 nm (see below), two rather intense bands are computed at 359 (oscillator strength $f = 0.024$) and 364 nm

Table 4. Electronic Absorption and Emission Data for Complexes **1**−**7** and **9**

complex	medium (T/K)	absorption λ_{max}/nm (ϵ_{max}/dm^3 mol^{-1} cm^{-1})	emission λ_{em}/nm[a] (τ_o/μs)
1	acetone (298)	264 (80 010), 296sh (72 800), 338sh (33 350)	533, 596sh (19.2)
	solid (298)		540, 601, 685sh[b] (<0.1)
	solid (77)		547, 615
2	acetone (298)	266 (80 380), 298sh (67 090), 336sh (36 200), 364sh (26 680)	531, 586sh (19.4)
	solid (298)		580, 655[b] (<0.1)
	solid (77)		530, 581, 655
3	acetone (298)	270 (86 430), 298sh (78 210), 338sh (41 210), 366sh (28 100)	524, 580sh (21.5)
	solid (298)		592, 676[b] (<0.1)
	solid (77)		520, 580
4	acetone (298)	264sh (46 350), 296sh (29 090), 344sh (10 710)	540, 600 (0.5)
	solid (298)		616[b] (15.2)
	solid (77)		655
5	acetone (298)	264 (85 297), 276sh (72 533), 356sh (11 287)	514, 579sh (0.4)
	solid (298)		538 (0.2)
	solid (77)		500
6	acetone (298)	270sh (74 210), 294sh (37 670), 314 (28 550), 334 (14 870)	479, 534, 602 (16.5)
	solid (298)		491, 542, 605 (<0.1)
	solid (77)		492, 550, 622
7	acetone (298)	266 (72 430), 298sh (47 410), 318sh (23 970), 340 (19080)	482, 538, 608 (19)
	solid (298)		539, 609 (<0.1)
	solid (77)		489, 538, 608
9[12a]	MeCN (298)	255sh (48 830), 305sh (32 390)	495 (6.5)[12a]
	acetone (298)		450, 540 (0.4)[12a]
	solid (298)		450, 530[12a]
	solid (77)		

[a] Excitation wavelength = 350 nm. [b] Excitation wavelength = 450 nm.

($f = 0.012$). They correspond to multiorbital mixed transitions from the HOMO region which is both carbon and metal in character to the LUMO region, in particular the LUMO + 2 which is, analogous to the LUMO and LUMO + 1 depicted in Figure 4, mainly carbon π^* in character. In agreement with a larger HOMO−LUMO gap with respect to that of the bis-diynyl complex model **5-H**, the calculated lowest electronic excitations of the mono-diynyl complex model **8-H** are shifted to higher energies. Four excitations are computed in the 309−315 nm region which might tentatively be assigned to the absorption band at 305 nm experimentally observed for the related parent molecule **9** (vide infra). Again they largely derived from the promotion of electrons from the HOMO region, in particular the HOMO and HOMO − 1, to the LUMO region. This clearly shows a significant dependence of the excitation energies upon the carbon chain length of the ligands in this kind of species.

Electronic Absorption and Emission Spectroscopy. The electronic absorption spectra of trinuclear copper(I) and silver(I) diynyl complexes **1**−**7** in dichloromethane are dominated by an intense absorption band at ca. 264−270 nm and absorption shoulders in the region of 296−366 nm. The high energy absorption bands at ca. 264−270 nm are ascribed to $\pi \rightarrow \pi^*$ (dppm) intraligand (IL) transition, since free dppm ligand also absorbs strongly in this region. The absorption shoulders at ca. 296−366 nm are likely to involve metal-perturbed $\pi \rightarrow \pi^*$ (C≡CC≡CR) transitions as suggested by TD-DFT calculations. The electronic absorption data are summarized in Table 4.

Excitation of solid state and fluid solutions of the trinuclear copper(I) and silver(I) diynyl complexes **1**−**7** with $\lambda > 350$ nm produced long-lived and intense luminescence. Their photophysical data are collected in Table 4. Vibronic structures with vibrational progressional spacings of ca. 1800−2200 cm^{-1} are observed for the diynyl complexes in both the solid-state and solution emission spectra, which are typical of the ν(C≡C) stretch in the ground state. This observation is suggestive of the involvement of the diynyl ligands in the excited state.

Possible assignments for the origin of these emissions in the trinuclear copper(I) and silver(I) diynyl complexes involve emissive states derived from ligand-centered [$\pi \rightarrow \pi^*$(C≡CC≡CR)] (IL) transition, metal-centered d → s transition or from either metal-to-ligand charge transfer (MLCT) or ligand-to-metal charge transfer (LMCT) transition. The long lifetime of the emissive state in the microsecond range exhibited by both the copper(I) and silver(I) diynyl complexes is suggestive of a triplet parentage.

The silver(I) diynyl complexes **6** and **7** were found to emit at higher energy than the corresponding copper(I) analogues **1** and **3**. A red shift in the emission energy of ca. 0.26 eV was observed from [$Ag_3(\mu$-dppm$)_3(\mu_3$-η^1-C≡C−C≡C−Ph$)_2$]PF_6 (**6**) ($\lambda_{max} = 479$ nm) to its copper(I) analogue, [$Cu_3(\mu$-dppm$)_3(\mu_3$-η^1-C≡C−C≡C−Ph$)_2$]PF_6 (**1**) ($\lambda_{max} = 533$ nm) in acetone solution. It is suggested that the possible origins for the observed red shift in energy from silver(I) to copper(I) involve states derived from either a metal-to-ligand charge transfer [d(M) → π^*(acetylide)] MLCT or a ligand-to-metal charge transfer [RC≡CC≡C$^-$ → Cu_3] LMCT transition. Copper(I) is much more easily oxidized, given the higher energy of the copper(I) 3d orbitals relative to those of the silver(I) 4d orbitals, and thus the MLCT energy for copper(I) should be lower than that for silver(I). However, the ionization energy of $Ag^+_{(g)}$ is nearly 10^4 cm^{-1} larger than that for $Cu^+_{(g)}$,[38] and thus an assignment of the emissive state as derived from a MLCT transition is less likely, given the relatively small energy difference for the emission of the trinuclear silver(I) diynyl complexes and their copper(I) analogues. The red shifts in the emission energy are in close resemblance with those observed in related systems,[12e] where an LMCT origin was proposed. For the related trinuclear

(38) (a) Moore, C. E. *Natl. Stand. Ref. Data Ser., (U.S. Natl. Bur. Stand.)* **1971**, *NSRDS-NBS, 35*, 51. (b) Moore, C. E. *Natl. Stand. Ref. Data Ser., (U.S. Natl. Bur. Stand.)* **1971**, *NSRDS-NBS, 35*, 116.

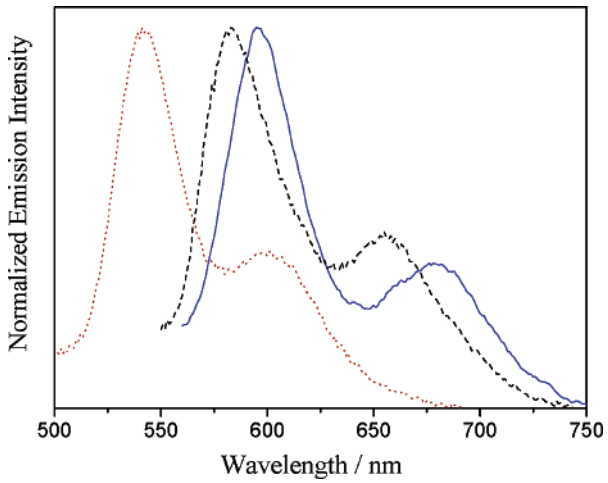

Figure 5. Normalized solid-state emission spectra of $[Cu_3(\mu\text{-dppm})_3(\mu_3\text{-}\eta^1\text{-C}\equiv\text{CC}\equiv\text{CR})_2]PF_6$ (R = Ph (**1**) (red ···), $C_6H_4-CH_3$-*p* (**2**) (black - - -), $C_6H_4-OCH_3$-*p* (**3**) (blue —)) at room temperature. Excitation wavelength at 450 nm.

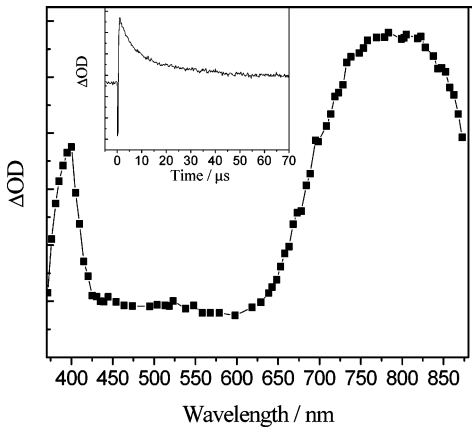

Figure 6. Transient absorption difference spectrum recorded 5 μs after the laser flash for a degassed acetone solution (0.1 M $^n Bu_4NPF_6$) of $[Cu_3(\mu\text{-dppm})_3(\mu_3\text{-}\eta^1\text{-C}\equiv\text{C}-\text{C}\equiv\text{C}-\text{Ph})_2]PF_6$ (**1**) (1×10^{-4} M) and 4-(methoxycarbonyl)-*N*-methylpyridinium hexafluorophosphate (3×10^{-3} M). The inset shows the decay trace of 4-(methoxycarbonyl)-*N*-methylpyridinly radical at 400 nm.

copper(I) and silver(I) monoynyl systems, a red shift in the 77 K solid-state emission of ca. 0.38 eV and ca. 0.29 eV on going from $[Ag_3(\mu\text{-dppm})_3(\mu_3\text{-}\eta^1\text{-C}\equiv\text{CPh})]^{2+}$ (λ_{max} = 428 nm)[12e] and $[Ag_3(\mu\text{-dppm})_3(\mu_3\text{-}\eta^1\text{-C}\equiv\text{CC}_6H_4\text{OMe-}p)]^{2+}$ (λ_{max} = 443 nm),[12e] respectively, to their corresponding Cu(I) analogues $[Cu_3(\mu\text{-dppm})_3(\mu_3\text{-}\eta^1\text{-C}\equiv\text{CPh})]^{2+}$ (λ_{max} = 492 nm)[12c] and $[Cu_3(\mu\text{-dppm})_3(\mu_3\text{-}\eta^1\text{-C}\equiv\text{CC}_6H_4\text{OMe-}p)]^{2+}$ (λ_{max} = 495 nm)[13c] was observed. Similarly a red shift in emission energy of ca. 0.27 eV on going from silver(I) to copper(I) chalcogenido clusters has been reported, in which a mixed d → s/LMCT origin has been suggested and supported by molecular orbital calculations.[13a,b] The assignment of a ^{3}MLCT origin is further disfavored by the observation that the solution emission energies of the aryl diynyl complexes **1**−**3** were found to be higher than that of the alkyl diynyl complex **4** for the copper series. Similarly, for the silver(I) diynyl complexes, the solution emission energy of **6** is slightly higher than that of **7**. The solid-state emission energies at room temperature also follow a trend of **5** > **1** > **2** > **3** > **4** for the copper complexes and **6** > **7** for the silver complexes. Figure 5 showed the solid-state emission spectra of complexes **1**−**3**. These trends are in line with the electron-donating ability of the diynyl ligands which is in the order: $^nC_6H_{13}$ > $C_6H_4OCH_3$ > $C_6H_4CH_3$ > Ph > H. Therefore, the origin of the emission has been proposed to involve substantial ligand-to-metal charge-transfer LMCT [diynyl → Cu_3] character. However, one should be aware that the assignments of electronic transitions between metal and/or ligand localized orbitals are only rough approximations because of the possible extensive orbital mixing in these complexes.

However, in view of the relatively short metal−metal distances found in the trinuclear copper(I) species, it is likely that the lowest-lying emissive state is mixed with some metal-centered character. When the emission energies of the diynyl complexes **1**, **3**, **4**, **6** and **7** are compared to those of their monoynyl analogues,[13d] a red shift is observed for the diynyl complexes that probably is a result of the slight increase in π-donating ability of the diynyl ligands and the involvement of an intraligand $\pi \rightarrow \pi^*$ character in the excited state. In view of the fact that the $\pi-\pi^*$ energy gap is lower for the diynyl ligands and the rich vibronic structures observed in the emission spectra of the diynyl complexes with vibrational progressional spacings typical of ν(C≡C) stretches, an involvement of a ligand-centered [$\pi \rightarrow \pi^*$(diynyl)] character in the emissive state of these complexes is suggested. This has been further supported by the molecular orbital calculations (vide supra). Similar assignment has also been suggested in the related trinuclear and hexanuclear d^{10} systems with highly conjugated, electron-deficient monoynyl and 1,4-diethynylbenzene type ligands, such as in $[M_3(\mu\text{-dppm})_3(\mu_3\text{-}\eta^1\text{-C}\equiv\text{C}-C_6H_4-NO_2\text{-}p)_n]^{(3-n)+}$ (M = Cu, Ag; *n* = 1, 2), $[Cu_3\{\mu\text{-}(Ph_2P)_2N-R\}_3(\mu_3\text{-}\eta^1\text{-C}\equiv\text{C}-C_6H_4-\text{Ph-}p)_2]^+$ (R = $CH_2CH_2CH_3$, Ph, $C_6H_4-CH_3$-*p*, C_6H_4—F-*p*),[12d] and $[M_3(\mu\text{-dppm})_3(\mu_3\text{-}\eta^1\text{-C}\equiv\text{C}-C_6H_2\text{-2,5-}R_2-\text{C}\equiv\text{C-}p)M_3(\mu\text{-dppm})_3]^{4+}$ (M = Cu, Ag; R = H, CH_3).[12f]

Photochemical Properties. Laser flash photolysis of a degassed acetone solution of **1** (1×10^{-4} M) and 4-(methoxycarbonyl)-*N*-methylpyridinium hexafluorophosphate (3×10^{-3} M) generated transient absorption bands at ca. 400 and 790 nm (Figure 6). The high-energy absorption band at ca. 400 nm is characteristic of the pyridinyl radical absorption.[39] With reference to previous spectroscopic work,[12b−d,13b−d] the broad intense absorption band at ca. 790 nm is likely to arise from the mixed valence $Cu^ICu^ICu^{II}$ species. The mechanism of the reaction is as follows:

$$[Cu_3(\mu\text{-dppm})_3(\mu_3\text{-}\eta^1\text{-C}\equiv\text{C-C}\equiv\text{C-Ph})_2]^+ + h\nu \rightarrow [Cu_3(\mu\text{-dppm})_3(\mu_3\text{-}\eta^1\text{-C}\equiv\text{C-C}\equiv\text{C-Ph})_2]^{+*}$$

$$[Cu_3(\mu\text{-dppm})_3(\mu_3\text{-}\eta^1\text{-C}\equiv\text{C-C}\equiv\text{C-Ph})_2]^{+*} + \text{(COOMe, N-Me pyridinium)} \rightarrow$$

$$[Cu_3(\mu\text{-dppm})_3(\mu_3\text{-}\eta^1\text{-C}\equiv\text{C-C}\equiv\text{C-Ph})_2]^{2+} + \text{(COOMe, N-Me pyridinyl radical)}$$

(39) (a) Hermolin, J.; Levin, M.; Kosower, E. M. *J. Am. Chem. Soc.* **1981**, *103*, 4808. (b) Hermolin, J.; Levin, M.; Ikegami, Y.; Sawayanagi, M.; Kosower, E. M. *J. Am. Chem. Soc.* **1981**, *103*, 4795.

Table 5. Electrochemical Data for the First Oxidation Couple of Complexes **1**−**7** and **9**

complex	oxidation[a] $E_{1/2}$/V vs SCE[b] (E_{pa}/V vs SCE)[c]
$[Cu_3(\mu\text{-dppm})_3(\mu_3\text{-}\eta^1\text{-C}\equiv\text{C}-\text{C}\equiv\text{C}-\text{Ph})_2]PF_6$ (**1**)	+0.81
$[Cu_3(\mu\text{-dppm})_3(\mu_3\text{-}\eta^1\text{-C}\equiv\text{C}-\text{C}\equiv\text{C}-\text{C}_6\text{H}_4\text{CH}_3\text{-}p)_2]PF_6$ (**2**)	+0.75
$[Cu_3(\mu\text{-dppm})_3(\mu_3\text{-}\eta^1\text{-C}\equiv\text{C}-\text{C}\equiv\text{C}-\text{C}_6\text{H}_4\text{OCH}_3\text{-}p)_2]PF_6$ (**3**)	+0.72
$[Cu_3(\mu\text{-dppm})_3(\mu_3\text{-}\eta^1\text{-C}\equiv\text{C}-\text{C}\equiv\text{C}-{}^n\text{C}_6\text{H}_{13})_2]PF_6$ (**4**)	+0.75
$[Cu_3(\mu\text{-dppm})_3(\mu_3\text{-}\eta^1\text{-C}\equiv\text{C}-\text{C}\equiv\text{C}-\text{H})_2]PF_6$ (**5**)	+0.88
$[Ag_3(\mu\text{-dppm})_3(\mu_3\text{-}\eta^1\text{-C}\equiv\text{C}-\text{C}\equiv\text{C}-\text{Ph})_2]PF_6$ (**6**)	(+1.10)
$[Ag_3(\mu\text{-dppm})_3(\mu_3\text{-}\eta^1\text{-C}\equiv\text{C}-\text{C}\equiv\text{C}-\text{C}_6\text{H}_4\text{OCH}_3\text{-}p)_2]PF_6$ (**7**)	(+1.19)
$[Cu_3(\mu\text{-dppm})_3(\mu_3\text{-}\eta^1\text{-C}\equiv\text{C}-\text{Ph})_2]PF_6$ (**9**)	+0.79[12a]

[a] In MeCN (0.1 M ^{n}Bu$_4$NPF$_6$), glassy carbon electrode, scan rate = 100 mV s^{-1}, 298 K. [b] $E_{1/2}$ is taken to be the average of E_{pa} and E_{pc}, where E_{pa} and E_{pc} are the anodic and cathodic peak potentials of the quasi-reversible oxidation couple, respectively. [c] E_{pa} is the anodic peak potential for the irreversible oxidation wave.

An extinction coefficient of 15 900 dm^3 mol^{-1} cm^{-1} was estimated for the broad absorption band at ca. 790 nm from a knowledge of the extinction coefficient of the pyridinyl radical species.[12b−d,13b−d] Similarly, recent transient absorption studies on the related trinuclear copper(I) monoynyl complexes also showed an intense low-energy band at ca. 790−810 nm.[12b,c] The relative insensitivity of the absorption energy of this band to the nature of the alkynyl ligand (monoynyl vs diynyl) is supportive of an assignment of an intervalence-transfer (IT) transition,

$$Cu^ICu^ICu^{II} + h\nu \rightarrow Cu^ICu^{II}Cu^I*$$

since the alkynyl ligands are bridging the metal centers in a $\mu_3-\eta^1$ bonding mode involving only a single carbon bridge.

The transient signal decays via second-order kinetics, with a back-electron-transfer rate constant, k_{bet} of 1.8×10^{10} dm^3 mol^{-1} s^{-1}, in line with the bimolecular nature of the back electron-transfer reaction.

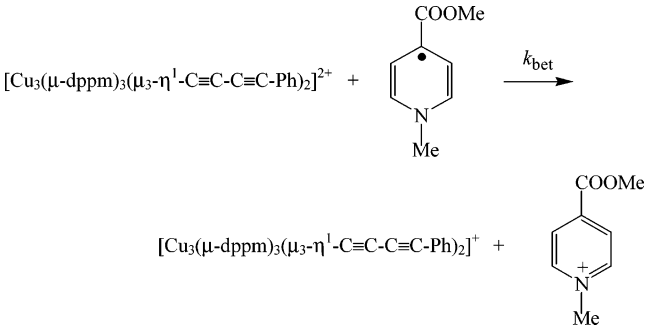

This provides direct spectroscopic evidence for the electron-transfer quenching mechanism for the bimolecular quenching reactions of the phosphorescent state with pyridinium acceptors. The decay trace of the transient absorption due to the pyridinyl radical at ca. 400 nm is shown in the inset of Figure 6.

Electrochemical Properties. The electrochemical properties of the diynyl complexes have also been studied. The electrochemical data from cyclic voltammetric studies of the complexes are summarized in Table 5.

The trinuclear copper(I) diynyl complexes show a quasi-reversible oxidation couple at +0.71 to +0.88 V vs S.C.E. Complexes with electron-rich diynyl ligands are found to be more easily oxidized, with the potential values **3** < **2** ≅ **4** < **1** < **5** for the trinuclear copper(I) bicapped diynyl complexes. This is supported by the IPs computed for the corresponding hydrogenated model complexes (vide supra). Initial examination of the trend would suggest an oxidation of either a metal-centered copper(I) to copper(II) oxidation or a diynyl ligand-centered oxidation. Since the trinuclear silver(I) diynyl complexes **6** and **7** did not show quasi-reversible oxidation couples at similar potentials as their respective copper(I) analogues, **1** and **3**, but rather an irreversible oxidation wave at ca. +1.2 V was observed, it is likely that the quasi-reversible oxidation couple in the copper(I) complexes has substantial metal-centered character but with mixing of some diynyl ligand-centered contributions. This is in agreement with the theoretical studies which indicate that some HOMOs are delocalized over the whole carbon ligand−metal triangle backbone. The diynyl complex **1** shows a very slightly more positive oxidation potential than its monoynyl counterpart **9**. Similar trends have also been observed with complexes **3** and **4** relative to their monoynyl counterparts, $[Cu_3(\mu\text{-dppm})_3(\mu_3\text{-}\eta^1\text{-C}\equiv\text{C}-\text{C}_6\text{H}_4-\text{OCH}_3\text{-}p)_2]^+$ ($E_{1/2}$ + 0.71 V vs. S. C. E.)[13c] and $[Cu_3(\mu\text{-dppm})_3(\mu_3\text{-}\eta^1\text{-C}\equiv\text{C-}{}^n\text{C}_6\text{H}_{13})_2]^+$ ($E_{1/2}$ +0.65 V vs S.C.E.),[13c] as supported by the IPs computed for the hydrogenated model complexes (vide supra).

Conclusion

A series of soluble trinuclear copper(I) and silver(I) complexes containing bicapped diynyl ligands, $[M_3(\mu\text{-dppm})_3(\mu_3\text{-}\eta^1\text{-C}\equiv\text{CC}\equiv\text{CR})_2]PF_6$ (M = Cu, R = Ph, $C_6H_4-CH_3$-*p*, $C_6H_4-OCH_3$-*p*, $^nC_6H_{13}$, H; M = Ag, R = Ph, $C_6H_4-OCH_3$-*p*), have been synthesized and characterized. The low-energy emission of these complexes has been assigned to be derived from states of substantial LMCT parentage, mixed with a metal-centered $nd^9(n+1)s^1$ state. Owing to the highly structured emission bands and the significantly long lifetimes, a possible involvement of a ligand-centered [$\pi \rightarrow \pi^*$(C≡CC≡CR)] excited state has not been ruled out.

Acknowledgment. V.W.W.Y. acknowledges support from The University of Hong Kong Foundation for Educational Development and Research Limited. The work described in this paper has been supported by a CERG grant from the Research Grants Council of the Hong Kong Special Administrative Region, China (Project No. HKU 7123/00P). C.H.L. and W.Y.L. acknowledge the receipt of postgraduate studentships, and N.Z. acknowledges the receipt of a university postdoctoral fellowship, both administered by The University of Hong Kong. S.F. and S.M. thank the French Ministry of Education and Research for postgraduate studentships. J.-F.H. thanks the Pôle de Calcul Intentif de l'Ouest (PCIO) of the University of Rennes for computing facilities. V.W.-W.Y. and J.-F.H. acknowledge the award of a travel grant by the RGC/CNRS under the PROCORE: Hong Kong−France Joint Research Scheme. J.-F.H. also thanks Dr. K. Costuas for helpful discussions.

Supporting Information Available: Crystallographic data for complexes **1** and **5**. The material is available free of charge via the Internet at http://pubs.acs.org.

JA049300X